Qualification Criteria for the Verification of Numerical Waves – Part 1: Potential-Based Numerical Wave Tank (PNWT)

Sébastien Fouques, Eloïse Croonenborghs, Arjen Koop, Ho-Joon Lim, Jang Kim, Binbin Zhao, Maxime Canard, Guillaume Ducrozet, Benjamin Bouscasse, Weizhi Wang, et al.

QUALIFICATION CRITERIA FOR THE VERIFICATION OF NUMERICAL WAVES – PART 1: POTENTIAL-BASED NUMERICAL WAVE TANK (PNWT)

Sébastien Fouques, Eloïse Croonenborghs
SINTEF Ocean
Trondheim, Norway

Arjen Koop
MARIN
Wageningen, The Netherlands

Ho-Joon Lim, Jang Kim[1]
Genesis
Houston, USA

Binbin Zhao
Harbin Engineering University
Harbin, China

Maxime Canard, Guillaume Ducrozet, Benjamin Bouscasse
Ecole Centrale de Nantes
Nantes, France

Weizhi Wang, Hans Bihs
NTNU
Norway

ABSTRACT

There is an increasing trend towards using numerical wave simulations for the design of offshore structures, especially for the stochastic prediction of nonlinear wave loads like those related to air-gap and wave impact. Unlike experimental facilities, where the complex nonlinear physics of wave propagation is simply enforced by the laws of nature, numerical wave tanks (NWTs) rely on assumptions and simplifications to solve the propagation equations in a reasonable amount of time. It is therefore important to verify the quality of the waves generated by NWTs in terms of realistic physical properties.

As part of the effort to develop reliable numerical wave modeling practices in the framework of the "Reproducible Offshore CFD JIP", qualification criteria are formulated for the wave solutions generated from either potential-flow based or CFD-based codes. The criteria have been developed based on experiences from physical wave tank tests and theoretical/numerical studies. They are being evaluated using results from several numerical models and available benchmark data. This paper presents the proposed qualification criteria and on-going evaluation efforts by comparing results from different codes.

INTRODUCTION

The mechanical generation of water waves in conventional experimental facilities can be hampered by the intrinsic boundary conditions of the laboratory. Wave reflection [1], spurious waves ([2], [3], [4], [5]) and eigenmodes [6] are typical issues researchers must deal with when assessing model responses during test campaigns. However, in such facilities, the complex nonlinear physics of wave propagation is simply enforced by the laws of nature. Numerical wave tanks (NWTs) face the opposite problem: boundary conditions can be flexible, but assumptions must be made, and shortcuts must be taken to be able to solve the propagation equations numerically in a reasonable amount of time. It is therefore important to check the quality of the waves generated by NWTs in terms of realistic physical properties.

In the frame of the "Reproducible Offshore CFD JIP", qualification criteria have been formulated to assess the quality of the waves generated numerically [7]. They are based on the work by [8] and [9], as well as on experience and best practice from various experimental test facilities. The purpose of these criteria is not to ensure that the numerical waves perfectly match known theories, but that their quality at least matches the quality of the waves generated experimentally for practical applications. In addition, they highlight some important

[1] Contact author: jang.kim@genesisenergies.com

physical aspects that need to be documented properly to better understand the computed responses.

The criteria proposed by the JIP are split into two categories depending on their purpose:

1. *Criteria to verify the quality of the waves obtained with a chosen numerical method and set-up.* Their purpose is to check well-known physical properties of some simulated waves. In case the proposed requirements are not met, the set-up and/or the method must be improved. Both regular and irregular waves are considered.
2. *Criteria to assess the quality of 3-hour wave realizations.* Here, the purpose is to check the quality of a single irregular wave realization against a specified target. If the criteria are not satisfied, the wave input and/or numerical set-up can be adjusted through an iterative process to achieve the required quality.

This paper focuses on the first set of criteria and irregular waves. After presenting the proposed criteria, as well as their practical implementation from postprocessed simulation results, the former is applied to various numerical wave tank codes based on potential-flow theory. The goal of this preliminary verification study is to assess the quality of the simulated waves, but also to verify whether the chosen qualification criteria are robust and practical.

Following [8], the numerical wave tank consists of a potential-NWT (PNWT) and a CFD-NWT (CNWT). This paper presents PNWT results while Part 2 [10] presents CNWT computations.

OVERVIEW OF NWT SIMULATIONS

The simulation domain of the CNWT is included in the simulation domain of the PNWT, as shown in Figure 1. Inside the CNWT-domain, the test area corresponds to the area where the quality of the waves must be assessed. Its size may depend on the type of application: it may be narrow for a fixed installation or wider for a moored structure with possible surge and sway motions. A reference point located at the center of the test area is defined.

The characteristic simulation domain parameters shown in Figure 1 are defined as follow:

- The simulated waves propagate along the positive x-axis.
- The PNWT domain starts at $x = 0$ and its length is L_{Pot}.
- The CNWT domain starts at $x = x_{CFD}$ and its length is L_{CFD}.
- The length of the test domain is L_{Test} and its center is located at $x = x_{Ref}$.

In addition to these parameters, set-up parameters include the size of the various meshes as well as the size of the coupling domains. The water depth is also considered as a set-up parameter since it is directly related to the vertical discretization of the domain.

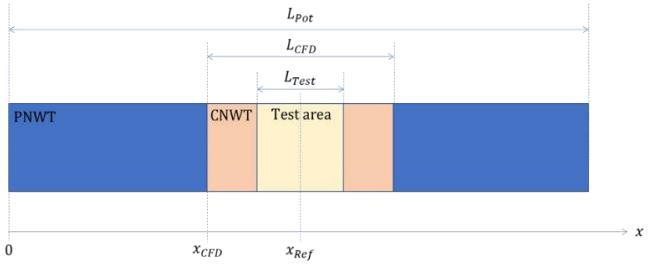

FIGURE 1: TWO-DIMENSIONAL SIMULATION DOMAIN. THE TEST AREA IS EMBEDDED IN THE CNWT DOMAIN, WHICH IS EMBEDDED IN THE PNWT DOMAIN. POSSIBLE OVERLAY ZONES FOR COUPLING ARE NOT REPRESENTED.

The criteria listed in the next section must be checked first with the PNWT, and then with the CNWT (without any structure). Although incoming waves are assumed to be long crested in the PNWT, the test area in the CNWT may be three-dimensional depending on the tested structure. In this case, the wave criteria have to be checked with the same three-dimensional domain and mesh as the one that will be used to study the tested structure.

Another important aspect is the PNWT-CNWT communication, which needs to be done with adequate format (see [10]).

GUIDELINE FOR NUMERICAL WAVE VERIFICATION (QUALIFICATION)

Stability and accuracy of irregular waves

The PNWT and CNWT must be able to generate 3-hour realizations of steep irregular waves from a specified spectrum. The numerical damping model used to deal with wave breaking in the PNWT should be robust enough to prevent the simulations from crashing. However, it should also be realistic enough to obtain correct extreme wave statistics with respect to surface elevation and kinematics. Moreover, for some applications in shallow water and intermediate depth, second-order low frequency (LF) excitations may be of importance. The PNWT and CNWT must therefore be able to generate LF-excitations in accordance with second-order wave theory.

Three-hour realizations of irregular waves shall be generated from one JONSWAP spectrum with a significant steepness $s_s \stackrel{\text{def}}{=} 2\pi H_s/(gT_P^2)$ equal to at least 0.03, and a peak enhancement factor γ=3. As an example, [8] used a significant wave height $H_s = 13.35m$ and a peak wave period $T_p = 17s$. For waves in intermediate depth and shallow water, the value of the steepness parameter can be reduced as for regular waves in the classification by [11]. The number of realizations should be at least 10, ideally 100 if the computing resource allows, to demonstrate the robustness of the code and to be able to derive

reliable ensemble statistics. In case random amplitudes and phases, and not only random phases, are used to initialize the spectral components (see Section 5.1 in [9]), one should expect a larger variability in the derived statistics.

Based on these irregular wave simulations, the following items must be verified.

Robustness check

The PNWT and CNWT should be able to generate all three-hour realizations without crashing. A main purpose of this criterion is to ensure that the numerical models can cope with wave breaking. Note that all realizations have to be simulated successfully with the same set-up in order to obtain consistent wave statistics.

Statistical and spectral parameters: homogeneity and sampling variability

The following properties are computed for each realization and for at least three positions throughout the test domain, and located at every $0.5\lambda_P$ or more frequent, including the reference position (λ_p standing for peak wave length):

- Spectral density *S(f)*
- Significant wave height H_S
- Spectral peak period T_P
- Skewness λ_3 and kurtosis λ_4 of the surface elevation.
- Crest height distribution.

It shall be documented that the properties above

- Do not depend on the position throughout the test area.
- Do not show outliers throughout the various realizations.
- Are consistent with the target values and simplified formulas, although these do not need to be matched accurately before a calibration procedure has been gone through.
- Are similar when estimated from the PNWT and the CNWT.

The skewness and kurtosis parameters characterize the nonlinearity of the surface elevation. For example, large kurtosis values are related to the occurrence of extreme waves [12]. They may show a large variability depending on the number of waves in the realization (see Section 5.3 in [9]), and their ensemble average over the various realizations should be used when checking the position dependency and for comparison purposes. For example, the following second-order approximations from [13] for water depth *h* can then be used as an indication for broad-banded spectra (see also the discussion on freak waves below):

$$\begin{aligned} \lambda_3 &= \frac{34.4H_S}{gT_P^2} + 2.14\times10^{-6}\left(\frac{gT_P^2}{h}\right)^3 \\ \lambda_4 &= 3+3\lambda_3^2 \end{aligned} \qquad (1)$$

However, for each individual realization, it must be checked that the obtained skewness and kurtosis values are physical, i.e., that $\lambda_3 > 0$ and $\lambda_4 > 3$ for deep-water waves. These conditions are related to the fact that nonlinear waves show flat troughs and sharp crests with an extreme values distribution that has a thicker tail compared to the gaussian one. Owing to sampling variability, an absolute tolerance of 0.04 and 0.15, for λ_3 and λ_4, respectively, can be accepted for a typical 3-hour realization with 500-1000 wave events (see Fig. 15 in [9]).

In addition, the sampling variability of H_S, λ_3 and λ_4 should be compared to the results given in Section 5.3 in [9].

Distribution of crest heights, horizontal particle velocity at the crests and crest front steepness

The distribution of the crest heights is derived for each realization as described for example in [14], along with the corresponding ensemble distribution. The latter distribution must be independent of the position in the test area and provide larger estimates for the crest heights than the second order Forristall distribution (see e.g. Section 3.5.10.4 in [15], [16]). Note that if the size of the test domain is large, the height of the largest crests may decrease as the waves propagate because of dissipation due to breaking. The crest height distributions can also be compared to the formulas given in [14] and [17] for the mean, as well as the upper 99th and lower 99th percentiles. These formulas are based on a regression analysis of nonlinear numerical simulations with JONSWAP spectra and peak enhancement parameters γ between 1 and 4. Consequently, they must be applied carefully for narrow-banded and steep spectra, i.e. with a large Benjamin-Feir index (BFI), for which nonlinear wave-wave interactions may enhance the probability of extreme crests.

The maximum horizontal particle velocity at the water surface is derived for each crest event described above. The obtained values must not be lower than the ones computed from second-order wave theory (see e.g. [18]). Note that low-pass filtering of the surface elevation may be necessary to derive second-order wave kinematics from nonlinear records, as mentioned in [15], Section 3.3.3.3.

The wave slope can be checked through the elevation rise velocity $\partial\eta/\partial t$ at a point in space. Since the nonlinear kinematic free surface conditions reads

$$\frac{\partial\eta}{\partial t} = w - u\frac{\partial\eta}{\partial x} \quad (z=\eta(x,t)), \qquad (2)$$

where η is wave elevation, u and w are the horizontal and vertical particle velocities at the free surface, respectively, the elevation rise velocity is a useful practical indicator for the local wave slope in steep waves. The crest front rate defined in Fig. 1 in [19] is a similar averaged parameter, which is more robust for noisy surface elevation signals. From laboratory experiences in steep sea states, the extreme values of $\partial\eta/\partial t$ should be expected to be up to 2 – 3 times the levels obtained

from linear wave theory. The most extreme cases correspond to breaking.

For a proper nonlinear reconstruction of random extreme wave events it is recommended to validate models against relevant experimental data, or to previously validated models, if available.

Second order low-frequency (LF) bound waves

For some applications in shallow water and intermediate depth, and when LF-excitations are relevant, the LF-part of the wave spectrum S(f) must be checked and compared to estimates from second-order theory. The typical relevant frequency range is from 0.005Hz to 0.02Hz in full scale (see e.g. Figure 7 in [8]).

The LF-spectral shape must be the same for all positions in each realization. If not, this may suggest the presence of spurious free-waves or LF-reflection (see [2], [3] and [5]).

Estimates from second-order wave theory can be obtained by band-pass filtering the surface elevation time series to extract a "linearized" part and reconstructing the second-order difference-frequency contribution [20].

In case one suspects the existence of spurious LF-waves, additional bi-chromatic waves can be simulated to better understand the nature of the LF-waves in the test area.

PNWT with periodic boundary conditions in space

Some PNWT, such as those based on the High Order Spectral method (see e.g. [21, 22, 23, 24]), use a simulation domain with periodic boundary conditions. In this case, the wave properties are uniform in space but their stability in time must be checked. The surface elevation and the velocity potential are generally initialized on the whole domain using linear wave theory, and nonlinearities are gradually incorporated by means of a ramp-up function as in [25]. For this type of PNWT, the homogeneity checks are replaced by stationarity ones: the time variation of the statistical and spectral parameters listed at the beginning of this section must be documented throughout the 3-hour simulations. For example, due to nonlinear wave-wave interactions, the shape of the spectrum may change during the simulation.

It must also be checked that the PNWT is able to derive the fluid velocity below large nonlinear crests, since the reconstruction algorithm may diverge (see e.g. Section I.3.2 in [26]).

Occurrence of freak waves for narrow-banded spectra

For moderately steep to steep long-crested or almost long-crested sea states with a narrow-banded spectrum, typically JONSWAP spectra with γ=3-5 and above, nonlinear modulation mechanisms are responsible for the generation of abnormally large waves in deep water. See for example [9], [27], [28] and [12]. Such modulation mechanisms require at least about 5 - 10 wave lengths to develop if the wave simulations are initialized with random linear waves, as it is usually done in laboratories, but also with some PNWT as shown e.g. in Fig. 2-4 in [27] and Fig. 19 in [28]. Consequently, the kurtosis of the surface elevation should in such cases be expected to strongly deviate from the values predicted by second-order theory. The governing parameter here is the Benjamin-Feir index (BFI), defined as the ratio of the wave steepness to the spectral bandwidth [27].

When such spectra and the occurrence of freak waves are relevant, it must be checked that the PNWT and CNWT are able to capture the non-linear mechanisms that can lead to the formation of abnormally large waves.

To do so, three sea states with BFI values increasing from 0.2 to 1.2, for example as the ones reported in [27], can be simulated. The kurtosis of the surface elevation computed at the reference position must then increase with the BFI. It should reach values above 3.6 for BFI=1.2, whereas it should be close to the value λ_4 given in Section 2.3 for BFI=0.2. If the waves are initialized with linear wave theory, the kurtosis should also increase with the distance x (see Figure 1) and then stabilize for $x \gtrapprox 5\ \lambda_P$, following the results presented in [27].

POST-PROCESSING

After a NWT simulation, selected output data and visualization images are archived as the record of the simulation. This section defines minimum recommended data and images that need to be archived to review the CFD simulation results.

The guidelines for the NWT data post-processing provided in this section is based on experience and best practice from various experimental test facilities on data processing of the wave signals from physical model test and numerical simulations.

Output Data and Post-Processing

- Time traces of the wave elevation should be monitored as function of time at certain locations.
- Plots of free-surface elevation in an animation or snapshots at different time-instants. For CNWT the free-surface elevation is defined as z-coordinate at the iso-surface defined by the void fraction being equal to 0.5.
- Velocity profile under a wave crest

Transient Time

Typically, a simulation is started from calm water with waves coming in at the inlet or from a prescribed wave solution based on linear theory. This initial solution will need time to develop to its fully developed stage. Therefore, for typical domain size, it is recommended not to include the first 1,200 s (full scale) of the simulation for the post-processing to remove any transient start-up effects. Therefore, for a 3-hour (10,800 s) simulation, the actual simulation time will be 12,000 s.

Surface Elevation, Steepness, and Rise Velocity

For CFD codes based on the volume of fluid (VOF) approach, the surface elevation η(x,y,z,t) is defined by the z-coordinate at which the void fraction is equal to 0.5 with respect to the calm water level. Note that in computational cells

the void fraction is calculated by solving the transport equation for the void fraction. Interpolation is required between the solutions in different computational cells to obtain the location where the void fraction is equal to 0.5. Most CFD codes have interpolation methods included to do this.

The rate of change $\partial\eta/\partial t$ of the free surface level needs to be calculated from the obtained free surface elevation signal by taking the derivative in time. One may have to use low-pass filtering to remove spikes which could result from the calculation of the time-derivative of a possibly noisy time series.

Wave Spectrum

The wave spectrum $S(f)$ is calculated from the time trace for the surface elevation. A direct FFT can be applied or a so-called WOSA (window overlapping spectral analysis) method can be applied to the 3-hour wave elevation time series measured at the target wave gauge. Spectrum smoothing is performed using convolution function. The smoothing window size is adjusted for 3-hour simulation between 50 and 100 for the wave conditions studied. Note that these values will depend on the sample duration of the simulation and bandwidth of the spectrum. A smaller window size is recommended for sharp spectrum (i.e. large γ in JONSWAP).

Significant Wave Height and Peak Wave Period

The significant wave height H_s and the peak wave period T_p are defined by

$$T_p = \frac{1}{f_p} \tag{3}$$

$$H_s = H_{m0} = 4\sqrt{M_0} \tag{4}$$

where f_p is the spectral peak frequency and where the spectral moment M_n is defined by

$$M_n = \int_0^\infty f^n S(f) df \tag{5}$$

Note that the significant wave height, H_s, can also be obtained as four times of the standard deviation of the surface elevation. Typically, these integrals are evaluated using the trapezoidal rule as these are the most robust way to integrate.

Extreme Values

The zero-crossing crest as shown in Figure 2 is used for the wave crest distribution. Note that low pass filter, usually standard 3-point or 5-point filtering, is applied to remove high frequency crossings in model test data. NWT results are usually clean for the surface elevation and no special treatment is necessary.

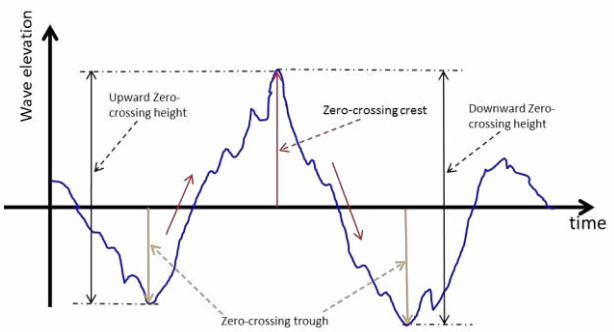

FIGURE 2: WAVE-CREST DEFINITION

Wave crest distribution

The wave crest data are sorted from lowest to highest values and probability of exceedance are calculated as: $Prob(n) = 1 - n/(N+1)$, where N is the total number of wave crest data and n is the index of specific wave crest in the sorted wave crest data.

The wave crest values versus the probability of exceedance is plotted (black diamonds in the figure). The red curve in the figure represents the 2nd order Forristall distribution [16]. In general, the Forristall distribution provides the lower bound of the 3-hour crest distribution for steep sea state.

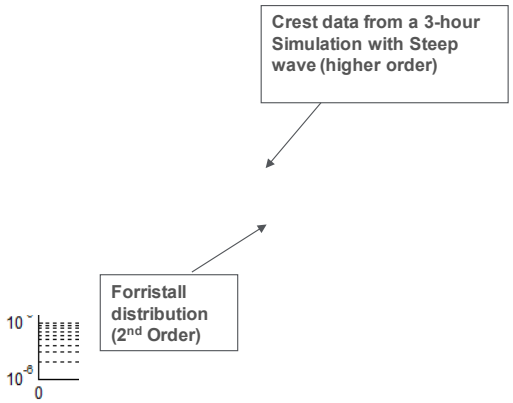

FIGURE 3: PROBABILITY DISTRIBUTION OF WAVE CRESTS

Skewness and Kurtosis

The skewness λ_3 and kurtosis λ_4 are defined as:

$$\lambda_3 = \frac{\mu_3}{\sigma^3}$$
$$\lambda_4 = \frac{\mu_4}{\sigma^4} \tag{6}$$

With μ_3, μ_4 and σ defined by

$$\mu_3 = E((X-\mu)^3)$$
$$\mu_4 = E((X-\mu)^4)$$
$$\sigma^2 = E((X-\mu)^2) \tag{7}$$

Where $\mu = E(X)$ is the mean value and E is the expectation operation or statistical average. X is wave elevation.

VERIFICATION RESULTS

Table 1 shows the two irregular wave conditions that are numerically simulated to verify NWT models based on the proposed qualification criteria. This paper (Part 1) presents the verification of PNWTs. Verifications of the CNWTs are presented in the Part 2 paper [10].

Table 2 shows the PNWT models that are tested for the verification of the 3-hour irregular wave simulation and the proposed qualification criteria. The purpose of this verification is not only to qualify PNWT, but also to verify whether the chosen qualification criteria are robust and practical. Preliminary acceptance criteria for each qualification criteria are proposed as references for the verification. The acceptance criteria are being finalized from the verification work presented in this paper and further verifications for more wave cases and PNWT [7].

TABLE 1: IRREGULAR WAVE CONDITIONS FOR NWT VERIFICATION

Case	Hs (m)	Tp (s)	Spectrum	γ
Case 1	6	12.25	JONSWAP	1.0
Case 3	17	15.50	JONSWAP	2.6

TABLE 2: PNWT MODELS FOR VERIFICATION

PWKS	Main Developer	Theory	Horizontal Approximation	Vertical Approximation
HOS-NWT [29, 30]	ECN	Potential Theory	Pseudo Spectral	Eigenfunction
HAWASSI [22]	LMI	Potential Theory, 3rd-order nonlinear	Pseudo Spectral	Eigenfunction
IGN [31, 32]	HEU	Stream-function Theory	Finite Difference	Polynomial
REEF3D::FNPF [33, 34, 35]	NTNU	Potential Theory	Finite Difference	Finite Difference
TPNWT [8]	TechnipFMC	Potential Theory	Finite Element	Polynomial

PNWT Model Setup

Simulations have been carried out for two wave conditions, Case 1 and Case 3, as shown in Table 1. Table 3 summarizes part of the numerical set up that was used for the simulations. Table 3 summarizes part of the numerical set up that was used for the verification cases of the PNWT models. Other details on the numerical scheme and wave breaking model are not covered in this paper and can be found at [8] and [29] for TPNWT and HOS-NWT, respectively.

All PNWT models apply linear wave kinematics, free-surface elevation and fluid velocity, at around inlet boundary to generate irregular wave inside the numerical domain. With the nonlinear physics modeled by the PNWT models the wave spectrum varies in space and successive corrections of input signal, either wave maker motion at inlet boundary for HOS-NWT [29] or forcing wave kinematics in overlay or relaxation zone for IGN, REEF3D and TPNWT [8], must be made to meet the criteria at the target location as done usually with experiments. In case of HAWASSI simulation, however, linear input wave kinematics derived from the target wave spectrum is forced at around the inlet boundary without further iterative corrections [8, 36]. Alternatively, nonlinearity in the HAWASSI model equations is gradually increased from zero (linear) at the inlet boundary to one (fully nonlinear) along the long transition zone. The different approaches in forcing explains the different distance from the inlet boundary and the starting locations of the nonlinear (NL) domain as shown in Table 3.

TABLE 3: PNWT SETUP PARAMETERS FOR VERIFICATION

	HAWASSI	HOS-NWT	IGN	REEF3D	TPNWT
Domain Length (m)	8200	5000	3500	5692.5	2750
NL Domain starts @ (m)	5000	0	390	900	300
Calibration Gauge @ (m)	5600	700	1700	3657.25	1500
NL Wave Propagation Distance (m)	600	700	1310	2757.25	1200
dx* (m)	4.00	12.50	3.00	1.65	2.00
dt (s)	0.165	0.033	0.03	0.045	0.06667

* In case of HAWASSI and HOS-NWT dx is the shortest wavelength in their spectral representation of the variables.

In all simulations, 10 wave gauges with 100 m spacing are put along the wave propagation direction. The fifth wave gauge, or WG5, is the calibration wave gauge where the H_s, T_p and wave spectrum are calibrated to match to the target values.

In total, 100 realizations are made for all wave conditions. All models did not show any numerical instabilities for all 12,000 sec simulations of 100 realizations. Initial HAWASSI simulations for Case 1 without wave-breaking model showed numerical instabilities for about 20 realizations out of 100 realizations. Case 1 was originally thought as a non-breaking case but breaking was observed when large number of realizations are made. When the breaking model was turned on, all 100 realizations could be simulated without any issues.

Summary of Case 1 Verification Results

Case 1 wave is the mild wave condition with negligible breaking events. All PNWT models could meet the qualification requirements of H_s, T_p and wave spectrum. The verification results from TPNWT and HAWASSI results are shown in this section. Both PNWT models could achieve the qualification with the linear input wave kinematics from the target spectrum without any corrections. As shown in Figure 4, the wave spectrum from TPNWT match the target spectrum within the 5% up to frequency $f = 0.18\,Hz$ (or $2.2\,f_p$). HAWASSI satisfies the criteria up $to\, f = 0.23\,Hz$ (or $2.8\,f_p$). At frequency higher than $0.2\,Hz$, TPNWT shows energy loss (lower wave energy than the input wave spectrum), whereas HAWASSI shows slightly increase in wave energy. This is presumably due to the numerical damping in TPNWT for wave components with short wavelength (or high frequency), which is typical in finite-difference or finite-

element based numerical methods. HAWASSI uses a spectral method that has less numerical damping than the other methods. A preliminary criterion for the wave spectrum (averaged over at least 100 realizations) is proposed as
"Spectral density $S(f)$ at calibration wave gauge should be within 5% of the target spectrum for all points within the following frequency range $f \in \left[\frac{3}{4T_P}, \frac{3}{2T_P}\right]$"

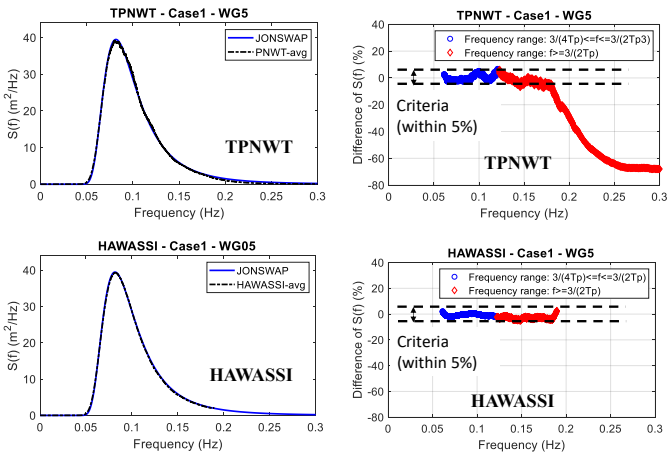

FIGURE 4: WAVE SPECTRUM (LEFT) AND RATIO BETWEEN SIMULATED AND TARGET SPECTRUM (RIGHT) FOR CASE1

Figure 5 shows the H_s, T_p, skewness and kurtosis from WG1 through WG10 from TPNWT and HAWASSI simulations. Both models show almost uniform H_s and T_p over the 10 wave gauges within 2% of the target value. Skewness shows minor variations around 0.15 for both models. The most variation is observed in the kurtosis. Both results show gradual increase of kurtosis from WG1 to WG5 and saturated kurtosis value after then. The wave propagation distances in the fully-nonlinear zone to reach the saturated kurtosis are $3\lambda_p$ and $6\lambda_p$ for HAWASSI and TPNWT, respectively. The faster saturation of kurtosis is observed in HAWASSI. The saturated kurtosis value from HAWASSI is slightly higher than the TPNWT results. But both values are significantly higher than the reference value shown in the figure, which is the approximate value from the second-order theory shown in Equation (1) and the reference value can be interpreted as a lower bound.

Figure 6 shows the crest height distribution from ensembled data from the 96 realizations. Forristall distribution from the 2nd-order theory and Huang's distribution from physical and numerical wave tank data are also compared. The $\pm 5\%$ range from Huang's distribution [14] [17], which is suggested as a preliminary qualification criterion, is also shown. Both TPNWT and HAWASSI show very good agreement with Huang's distribution. TPNWT shows crest height slightly higher than HAWASSI. When the rise velocity of the wave elevation is compared, TPNWT shows higher value as shown in Figure 7. For the wave-elevation rise velocity, there is no available benchmark for Case 1. The difference in the rise velocity will be revisited in the next section for Case 3, for which the benchmark data from the model test is available.

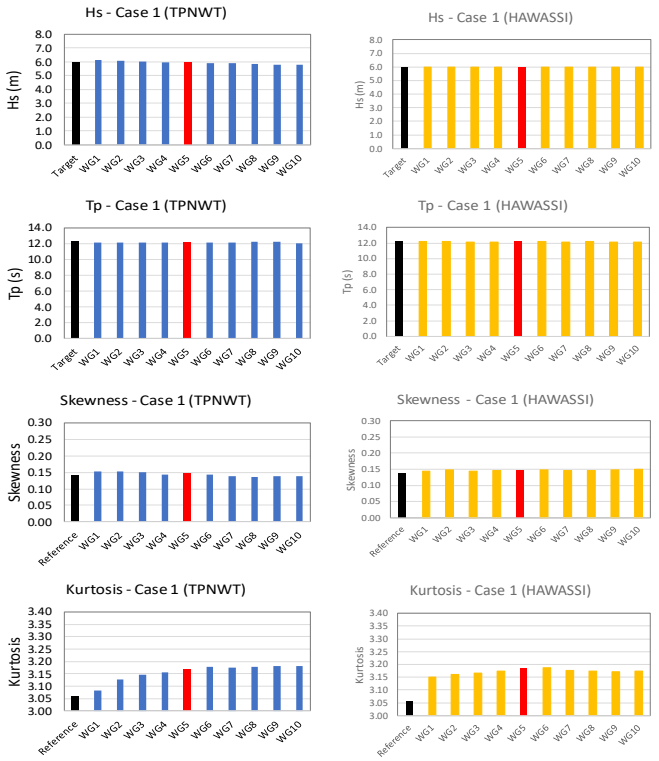

FIGURE 5: H_S, T_P, SKEWNESS AND KURTOSIS AT WAVE GAUGES (WG1 – WG10) FOR CASE1

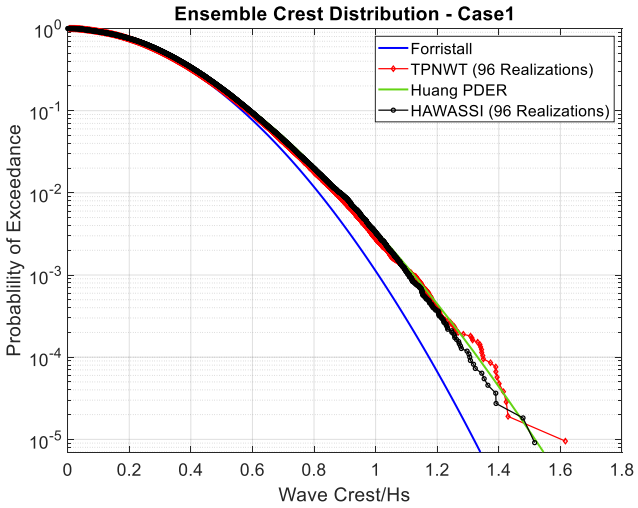

FIGURE 6: ENSEMBLE PROBABILITY DISTRIBUTION OF CREST HEIGHT FOR CASE1

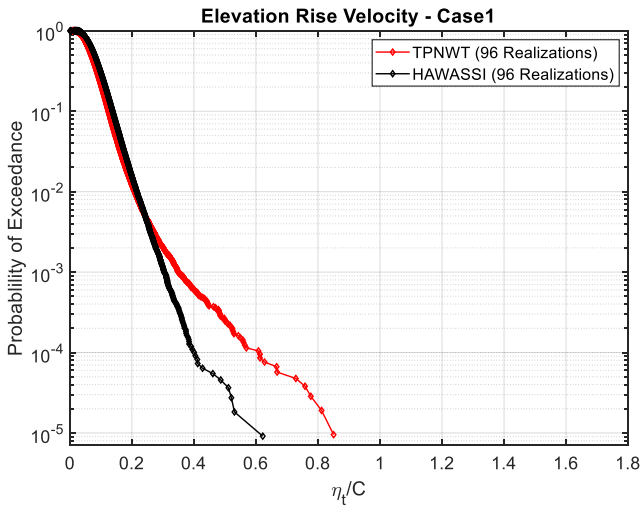

FIGURE 7: ENSEMBLE PROBABILITY DISTRIBUTION OF WAVE-ELEVATION RISE VELOCITY FOR CASE1

Summary of Case 3 Verification Results

Case 3 wave is the steep wave case with severe breaking. Iterative calibration scheme of input wave had to be used to meet the H_s, T_p and wave spectrum requirement for HOS-NWT, IGN, REEF3D and TPNWT. HAWASSI used the linear input wave without correction. Model test data from 8 realizations are also compared. As shown in Figure 8, the wave spectrum from model test model test does not satisfy the 5% criteria but may satisfy the relaxed requirement of 10%. HOS-NWT and TPNWT satisfy the 5% criteria.

Figure 9 shows the H_s, T_p, skewness and kurtosis from WG1 through WG10 from PNWT simulations. Model test values at the calibration wave gauge, WG5, are also shown for comparison. All PNWT models except HOS-NWT showed H_s over the 10 wave gauges within the 5% of the target value. But HOS-NWT model gives H_s within 5% bound from the WG6. The higher rate of Hs reduction along the wave gauges explains the higher Hs at the WG1 through WG5. Please note that different wave-breaking models of their own are used in different PNWT models and calibration of the wave-breaking models are not attempted yet for this verification study. All PNWT models showed uniform T_p over the 10 wave gauges, within the 1% of the target values. Skewness and kurtosis from all PNWT models stay within 10% deviation from the average values, which is close to the 2nd-order reference values. All models show gradual increase of kurtosis from WG1 to WG10. HAWASSI results show saturated kurtosis value earlier than other PNWT models. The saturated kurtosis values from IGN and TPNWT are close to the saturated HAWASSI value. HOS-NWT and REEF3D shows lower and higher kurtosis values than the other models, respectively.

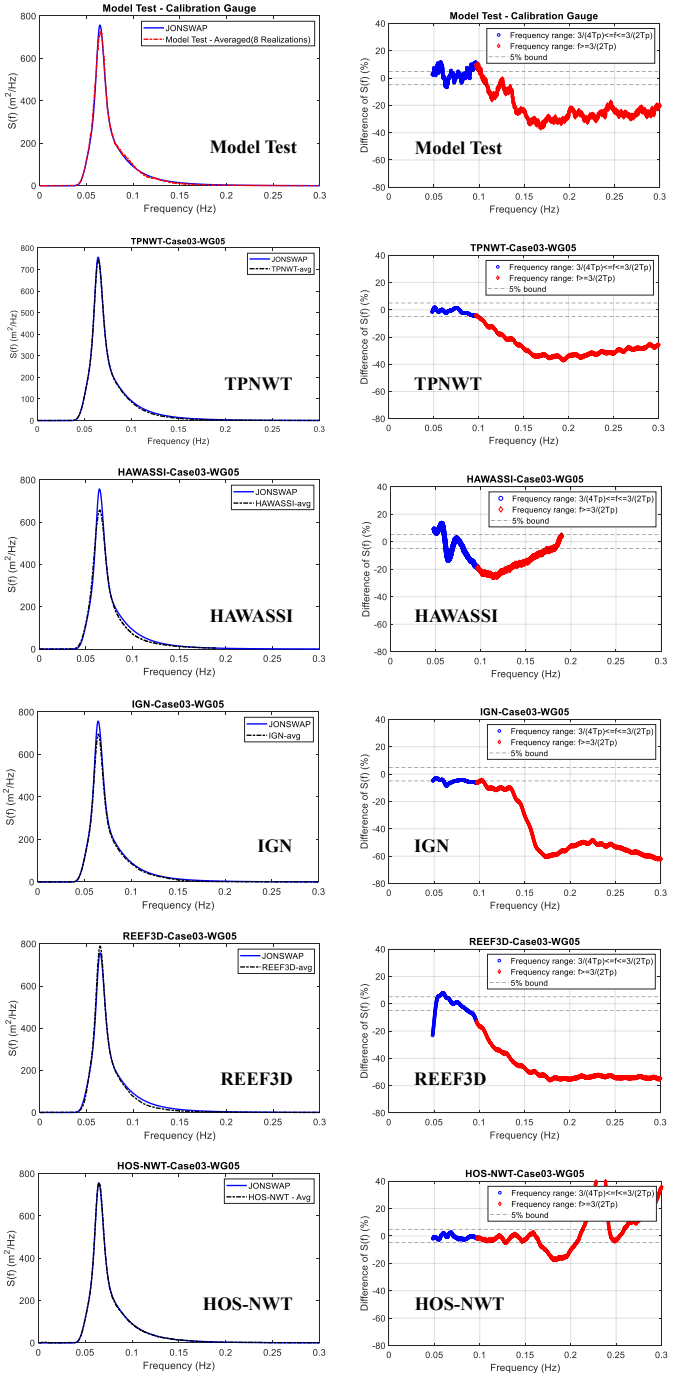

FIGURE 8: WAVE SPECTRUM (LEFT) AND RATIO BETWEEN SIMULATED AND TARGET SPECTRUM (RIGHT) FOR CASE3

Figure 10 shows the crest height distribution from ensembled data from 100 realizations are compared with the three (3) empirical formula:

1. Forristall distribution from the 2nd-order wave theory [16]
2. Huang's PDSR distribution from single 3-hour realizations [14] [17]

3. Huang's PDER distribution from ensemble of 3-hour realizations [17]

It is interesting to note the common trends in the variations among the PNWT models in kurtosis and wave crest distribution. HAWASSI, IGN and TPNWT, which showed close kurtosis values each other in Figure 9 also show close wave crest distribution as shown in Figure 10. They lie in between Forristall and PDER distribution. HOS-NWT and REEF3D results show wave crest distribution close to Forristall and PDSR distributions, respectively. From these trends, it is also observed that the wave kurtosis and wave crest distribution are correlated to the nonlinear wave propagation distance shown in Table 3. For example, the REEF3D model has the longest nonlinear wave propagation distance (i.e. 2757.25m) and the largest kurtosis and crest distribution. On the other hand, HOS-NWT has the shortest nonlinear wave propagation distance (i.e. 700m) and the smallest kurtosis and wave crest distribution. Note that the nonlinear wave propagation distance in the HAWASSI model is 600m, but it has extremely longer transition zone (i.e. 5000m) than other models as shown in Table 3. Similar trends have been observed in the physical model tests from different basin sizes. Further investigations on the dependency between wave propagation distance and wave-crest distribution are on-going.

Figure 11 shows the probability distributions of the peak rise velocity of the wave elevation. More scatter of the data from PNWT models is observed than the crest distribution shown in Figure 10. HAWASSI and IGN models, which showed closer wave crest distribution to the TPNWT, show significantly lower rise velocity value than TPNWT but close to the HOS-NWT value. The rise velocity distribution from the model tests is also presented as a reference. Note that model tests data are presented after applying low-pass filters with three different cut-off frequencies (infinity, 1.2 Hz and 0.7 Hz). Model test data for breaking waves typically contain high frequency noise due to air entrainment and capillary effects. The rise velocities are very sensitive to the cut-off frequency of the low-pass filter. In case of PNWT results, the rise velocity could be sensitive to mesh size as well as the simplified wave breaking model used in the simulations. Further comparisons with consistent mesh size among the PNWT models are recommended.

CONCLUSIONS

As a first step to establish the CFD modeling practices for the fully nonlinear irregular waves in the frame of the "Reproducible Offshore CFD JIP", qualification criteria for the wave models and the waves generated by the wave models are proposed in this paper. The criteria are applied to number of potential-based wave models listed in Table 2.

The following qualification criteria are applied for the verification:

- Spectral density *S(f)*
- Significant wave height H_S
- Spectral peak period T_P
- Skewness λ_3 and kurtosis λ_4 of the surface elevation
- Probability distribution of crest height
- Probability distribution of crest rise-velocity

The first three criteria are to confirm the reproduction of the prescribed wave energy spectrum. The preliminary verification results presented in this paper have been used to determine preliminary acceptance criteria. The acceptance criteria are further refined from the verification of more sea states and PNWTs.

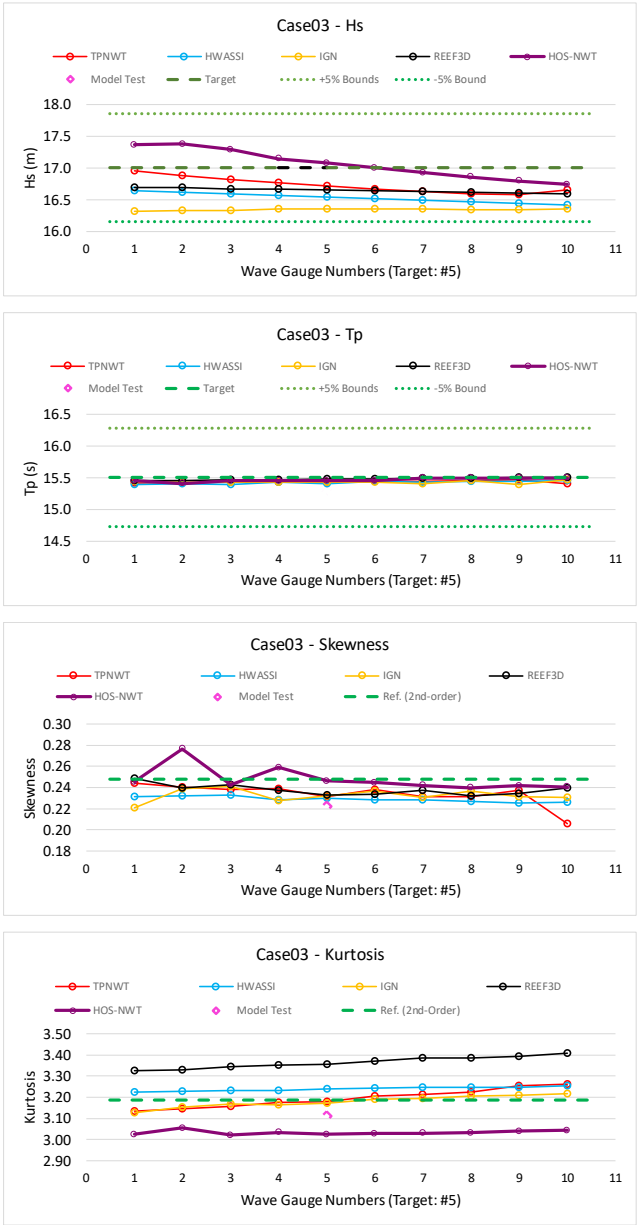

FIGURE 9: HS, TP, SKEWNESS AND KURTOSIS AT WAVE GAUGES (WG1 – WG10) FOR CASE3

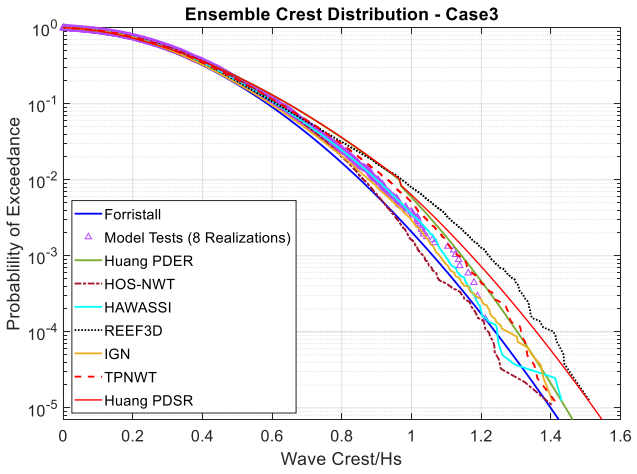

(a) Comparison of ensemble crest distribution

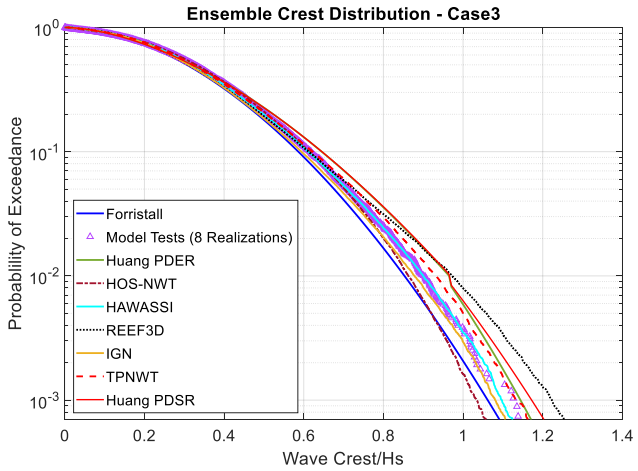

(b) Ensemble crest distribution - probability up to $7x10^{-4}$

FIGURE 10: ENSEMBLE PROBABILITY DISTRIBUTION OF CREST HEIGHT FOR CASE3

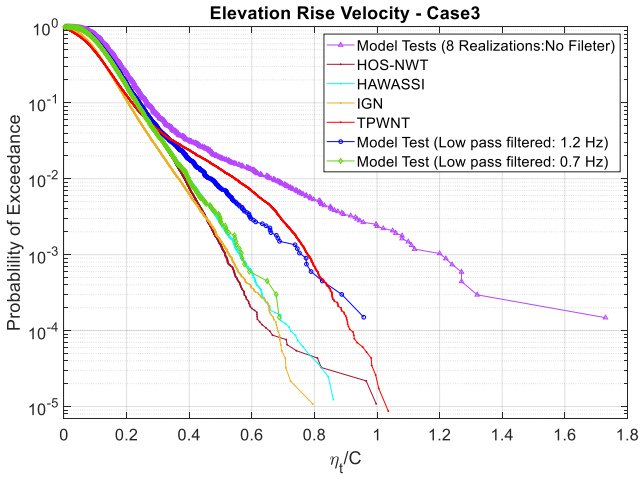

FIGURE 11: ENSEMBLE PROBABILITY DISTRIBUTION OF WAVE-ELEVATION RISE VELOCITY FOR CASE3

For the remaining criteria, the available theoretical and empirical values are applied as candidates for the acceptance criteria. The following findings are made:

1. The skewness and kurtosis from the second-order potential theory can be used as reference values for lower-bounds
2. Kurtosis can be a good indicator to confirm the sufficient wave-propagation distance for fully-developed nonlinear wave kinematics
3. The Forristall distribution, empirical formula from the second-order potential model, can be used as a reference value for lower-bound for the crest height distribution
4. The Huang's PDER distribution, empirical formula from the fully-nonlinear potential wave model, showed promising potential to be used as the acceptance criteria for the crest height distribution; this has to be confirmed with more model tests results.
5. The nonlinear wave models agreed well with each other for all qualification criteria other than the probability distribution of crest elevation and crest rise velocity.
6. The probability distribution of crest elevation from nonlinear wave models for the severe breaking case (Case 3, $H_s = 17\,m$, $T_p = 15.5\,s$) lies in between Forristall distribution as the lower bound and Huang's PDSR distribution as the upper bound, except the HOS-NWT and REEF3D.

Preliminary acceptance criteria for the qualification of the numerical waves are established based on the findings. The criteria are being refined the Workgroups in the Reproducible Offshore CFD JIP by

1. Verification of numerical waves generated by CNWT [10]
2. Application of the same criteria on the model test data with enough, at least 10, realizations
3. Consolidation of the parameters for wave breaking models.

ACKNOWLEDGEMENTS

The authors are grateful to the members of the "Reproducible Offshore CFD JIP", who approved the publication of this paper. Also appreciated is TechnipFMC Offshore Global Business Unit for their partial financial support for the JIP.

REFERENCES

[1] J. A. Zelt and J. E. Skjelbreia, "Estimating incident and reflected wave fields using an arbitrary number of gauges," in *Proc. Coastal Engineering*, Venice, Italy, 1992.

[2] C. T. Stansberg, "Laboratory modelling for floating structures in shallow water," in *Proc. OMAE2006-92496*, Hamburg, Germany, 2006.

[3] M. Naciri, T. Bunnik, B. Buchner and R. H. M. Huijsmans, "Low frequency motions of LNG carriers moored in shallow water," in *Proc. OMAE2004-51169*, Vancouver, BC, Canada, 2004.

[4] H. A. Schäffer, "Second-order wave maker theory for irregular waves," *J. of Ocean Engineering,* vol. 23, no. 1, pp. 47-88, 1996.

[5] N. Fonseca, G. Tahchiev, C. T. Stansberg, S. Fouques and M. Rodrigues, "Model tests and numerical prediction of the low-frequency motions of a moored ship in shallow water with a wave splitting method," in *39th International Conference on Ocean, Offshore and Arctic Engineering, OMAE2020-18806*, Fort Lauderdale, FL, USA, 2020.

[6] S. van Essen, W. Pauw and J. van der Berg, "How to deal with basin modes when generating irregular waves on shallow water," in *Proc. OMAE2016-54134*, Busan, South Korea, 2016.

[7] J. Kim and H.-J. Lim, "JIP on Reproducible CFD Modeling Practices for Offshore Applications. NWT Preparation Workgroup Year 1 Report, Rev. H.," TechnipFMC, 2019.

[8] A. Baquet, J. W. Kim and J. Huang, "Numerical modeling using CFD and potential wave theory for three-hour nonlinear irregular wave simulations," in *Proc. OMAE2017-61090*, Trondheim, Norway, 2017.

[9] C. T. Stansberg, "Analysis of Random Waves in Ocean Engineering," in *Marine Technology and Engineering, C. Guedes Soares et al.*, London, UK, CRC/Taylor & Francis, 2011.

[10] B. Bouscasse, A. Califano, Y. M. Choi, X. Haihua, J. W. Kim, Y. J. Kim, S. H. Lee, H. J. Lim, D. M. Park, M. Peric, Z. Shen and S. Yeon, "Qualification criteria and the verification of numerical waves - Part2: CFD-based numerical wave tanks," in *Proc. OMAE2021-63710*, Vurtual, Online, 2021.

[11] B. Le Méhauté, An introduction to hydrodynamics and water waves, Springer, 1976.

[12] N. Mori and P. A. E. M. Janssen, "On kurtosis and occurrence probability of freak waves," *J. Phys. Oceanogr. 36,* pp. 1471-1483, 2006.

[13] T. Vinje and S. Haver, "On the non-Gaussian structure of ocean waves," in *Seventh International Conference on the Behaviour of Offshore Structures (BOSS)*, Cambridge, MA, USA, 1994.

[14] J. Huang and Q. Guo, "Semi-empirical crest distribution of long crest nonlinear waves of three-hour duration," in *Proc. OMAE2017-61226*, Trondheim, Norway, 2017.

[15] DNVGL-AS, Recommended Practice DNVGL-RP-C205, Environmental conditions and environmental loads, 2017.

[16] G. Z. Forristall, "Wave Crest Distributions: Observations and Second Order Theory," *Journal of Physical Oceanography,* vol. 30, pp. 1931-1943, 2000.

[17] J. Huang and Z. Y, "Semi-emprical single realization and ensemble crest distribution of long crest nonlinear waves," in *Proc. OMAE2018-78192*, Madrid, Spain, 2018.

[18] C. T. Stansberg, O. T. Gudmestad and S. K. Haver, "Kinematics under extreme waves," *Journal of Offshore Mechanics and Arctic Engineering,* vol. 130, no. 2, 2008.

[19] E. M. Bitner-Gregersen, K. J. Mørk and C. T. Stansberg, "Extreme steepness of numerical model and laboratory waves," in *Fifth International Offshore and Polar Engineering Conference, ISOPE*, The Hague, The Netherlands, 1995.

[20] T. Marthinsen and S. R. Winterstein, "On the skewness of random surfaces," in *Proc. of Second International Offshore and Polar Engineering Conference (ISOPE)*, San Francisco, CA, USA, 1992.

[21] D. G. Dommermuth and D. K. P. Yue, "A high-order spectral method for the study of nonlinear gravity waves," *J. Fluid Mech.,* vol. 184, pp. 267-288, 1987.

[22] G. Klopman, B. Van Groesen and M. W. Dingemans, "A variational approach to Boussinesq modelling of fully nonlinear water waves," *Journal of Fluid Mechanics,* vol. 657, pp. 36-63, 2010.

[23] B. J. West, K. A. Brueckner, R. S. Janda, D. M. Milder and R. L. Milton, "A new numerical method for surface hydrodynamics," *J. Geophys. Res.,* vol. 92, no. (C11), pp. 11803-11824, 1987.

[24] G. Ducrozet, F. Bonnefoy, D. Le Touzé and P. Ferrant, "HOS-ocean: Open-source solver for nonlinear waves in open ocean based on High-Order Spectral method," *Computer Physics Communications,* vol. 203, pp. 245-254, 2016.

[25] D. G. Dommermuth, "The initialization of nonlinear waves using an adjustment scheme," *Wave Motion,* vol. 32, pp. 307-317, 2000.

[26] G. Ducrozet, "Modélisation des processus non-linéaires de génération et de propagation d'états de mer par une approche spectrale.," École Centrale de Nantes. tel-00263596, 2008.

[27] M. Onorato, A. R. Osborne, M. Serio and L. Cavalieri, "Modulational instability and non-Gaussian statistics in experimental random water-wave trains," *Phys. Fluids,* vol. 17, pp. 078101-4, 2005.

[28] M. Onorato, L. Cavalieri, S. Fouques, O. Gramstad, P. A. E. M. Janssen, J. Monbaliu, A. R. Osborne, Pakozdi C., M. Serio, C. T. Stansberg, A. Toffoli and K. Trulsen, "Statistical properties of mechanically generated surface gravity waves: a laboratory experiment in a three-dimensional wave basin," *J. Fluid Mech. 627,* pp. 235-257, 2009.

[29] M. Canard, G. Ducrozet and B. Bouscasse, "Generation of 3hr long crested waves of extreme sea states with HOS-NWT solver," in *Proc. OMAE2020-18930*, Virtual, Online, 2020.

[30] G. Ducrozet, F. Bonnefoy, D. Le Touze and P. Ferrant, "A modified high-order spectral method for wavemaker modeling in a numerical wave tank," *Journal of Mechanics-B/Fluids,* vol. 34, pp. 19-34, 2012.

[31] J. W. Kim and R. C. Ertekin, "A numerical study of nonlinear wave interaction in regular and irregular seas: irrotational Green-Naghdi model," *Marine Structure,* vol. 13, pp. 331-347, 2000.

[32] W. C. Webster and B. Zhao, "The development of a high-accuracy, broadband, Green-Naghdi model for steep, deep-water ocean waves," *Journal of Ocean Engineering and Marine Energy,* 2018.

[33] H. Bihs, A. Kamath, C. M. Alagan, A. Aggarwal and Ø. A. Arntsen, "A New Level Set Numerical Wave Tank with Improved Density Interpolation for Complex Wave Hydrodynamics," *Computers & Fluids,* vol. 140, no. DOI: 10.1016/j.compfluid.2016.09.012, pp. 191-208, 2016.

[34] H. Bihs, C. M. Alagan, A. Kamath and Ø. A. Arntsen, "Numerical investigation of focused waves and their interaction with a vertical cylinder using REEF3D," *Journal of Offshore Mechanics and Arctic Engineering,* vol. 139(4), no. 041101, 2017.

[35] H. Bihs, W. Wang, C. Pakozdi and A. Kamath, "REEF3D::FNPF – A Flexible Fully Nonlinear Potential Flow Solver," *Journal of Offshore Mechanics and Arctic Engineering,* vol. 142(4), no. DOI: 10.1115/1.4045915, 2020.

[36] B. Bouscasse, G. Ducrozet, J. W. Kim, H. J. Lim, Y. M. Choi, A. Bockman, C. Pakozdi, E. Croonenborghs and H. Bihs, "Development of a protocol to couple wave and CFD solvers towards reproducible CFD modeling practices for offshore applications," in *Proc. OMAE2020-10654*, Virtual, Online, 2020.